Rev. Adv. Mater. Sci. 33 (2013) 402-410

NUMERICAL SIMULATION OF TEMPERATURE FIELD AND STRESS DISTRIBUTIONS IN MULTI-PASS SINGLE-LAYER WELD-BASED RAPID PROTOTYPING

H. H. Zhao, H.C. Li, G. J. Zhang, Z. Q. Yin and L. Wu

State Key Laboratory of Advanced Welding and Joining, Harbin Institute of Technology, Harbin 150001, China

Received: October 17, 2011

Abstract. The complicated temperature field distribution during multi-pass single-layer weld-based rapid prototyping induces complex thermal stress evolutions and residual stress distributions. In this paper, a three-dimensional finite element model with temperature-dependent material properties is presented to investigate the temperature field and thermal stress distributions in multi-pass single-layer weld-based rapid prototyping. The experiments of multi-pass single-layer weld-based rapid prototyping are carried out to measure the thermal cycles and residual stress distributions of the depositing component. The results show that the variation trends of simulated results are in agreement with the experimental results. In the depositing process of multi-pass single-layer weld-based rapid prototyping, the rear pass has the stress release effect on the fore passes, and the non-uniform multi-peak thermal cycle experienced during the depositing is the main cause of the stress release effect. The stress of the last pass plays a significant effect on the residual stress distribution of the whole component.

1. INTRODUCTION

The weld-based rapid prototyping has become an increasingly interested manufacturing technology because of the advantages of the high production efficiency, the low cost, excellent properties, the high density and the good bonding strength [1]. Recently, researches on the establishment of the weld-based rapid prototyping system, the implementation of the fabrication process, and the distortion regularity of components have been conducted [1-4]. Additionally, in weld-based rapid prototyping process, components undergo complicated thermal cycles, which will result in the complex stress evolutions and distributions.

Currently, one of the most significant discussions in the field of rapid prototyping is about the thermal process, stress evolutions and residual stress distributions. The researches on the thermal processes [5-8] and thermal stress distributions [8,9] of rapid prototyping using laser as the depositing heat source has been widely researched. Dai and Shaw [5] adopted the finite element method to simulate the rapid prototyping process using a moving laser beam as the depositing heat source and investigate the temperature field, thermal and residual stresses and distortions of the component. It was shown that the process parameters had a significant influence, and the residual stress and distortion increased with the increase of the laser-scanning rate. Alimardani et al. [8] presented a finite element model of laser solid freeform fabrication process for the investigation of the temperature field, thermal stress distributions, and the effects of pre-heating and clamping the component on thermal stress distributions. Nickel et al. [9] studied the effect of deposition patterns for beam substrates

Corresponding author: G. J. Zhang, e-mail: zhanggj@hit.edu.cn

and plate substrates on residual stresses and deflections of laser deposited metal parts. Results showed that deposition patterns on substrates with different shapes had an important effect on the stress distributions and deflections of the parts. Additionally, the thermal process and stress distributions during welding processes have been widely investigated using finite element method [10,11]. However, the quantity of researches on the temperature field and stress distributions in the deposition of weld-based rapid prototyping is limited.

In present study, a three-dimensional thermal-mechanical coupled numerical model with temperature-dependent material properties is presented to investigate the temperature field, thermal cycles, temperature gradients, stress evolutions and stress distributions of multi-pass single-layer weld-based rapid prototyping. Meanwhile the multi-pass single-layer weld-based rapid prototyping experiment is carried out. Simulation results of thermal cycles and residual stresses are compared with the experimental measurements to verify the numerical model presented.

2. WELD-BASED RAPID PROTOTYPING EXPERIMENT

Multi-pass single-layer weld-based rapid prototyping experiment was carried out to investigate the thermal cycles and residual stress distributions at concerned locations. The mild steel plates S235JR (200×120×10 mm^3) was used as the substrate, and filling material was H08Mn2Si. The rapid prototyping component is shown in Fig. 1. The direct current gas metal arc welding (GMAW) was used to deposit, and ten passes of depositing metal with the length of 150 mm were deposited on the substrate. The depositing speed is 1.67 mm s^{-1}, the voltage is 18.1 V, and the current is 135 A. As shown in Fig. 2, every two adjacent passes were reversely deposited. The thermal cycles on the substrate were measured by thermocouples (K type) located at the points A, B, C, and D on the top and bottom surfaces of the substrate. The residual stresses were measured in the hole-drilling strain-gage method. The positions of strain gauges are shown in Fig. 3.

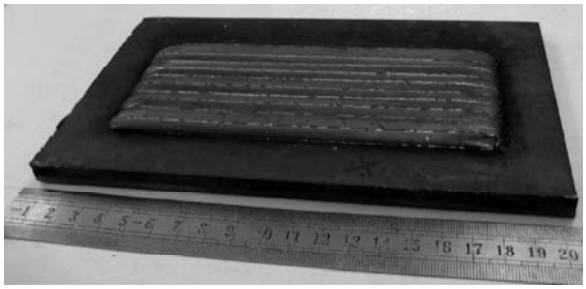

Fig. 1. Weld-based rapid prototyping component.

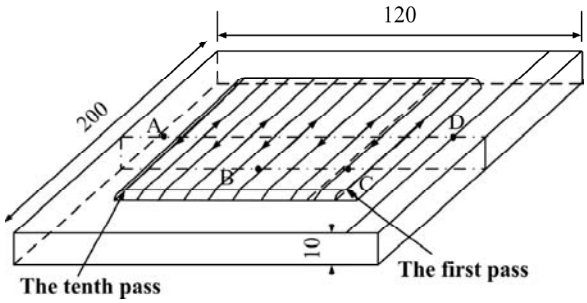

Fig. 2. Distributions of thermocouples.

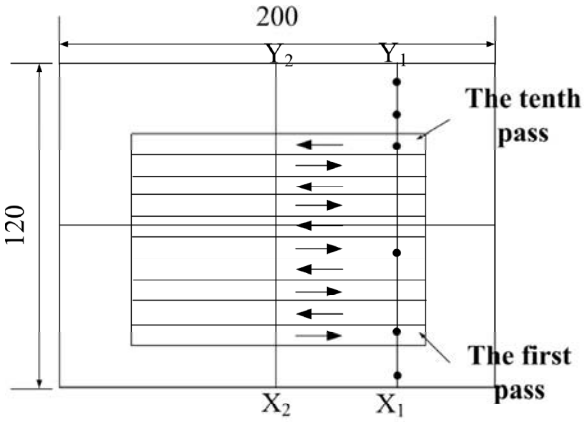

Fig. 3. Distributions of strain gauges.

3. THREE-DIMENSIONAL FINITE ELEMENT MODEL

Using the simulation software MSC.Marc, a three-dimensional elastic-plastic finite element model of ten-pass single-layer rapid prototyping is presented to study the temperature field and thermal stress distributions. The finite element model presented is shown in Fig. 4, and the total number of elements and nodes used are respectively 26078 and 30147. *X* direction stands for the width direction, *Y* direction is the thickness direction, and *Z* direction is the depositing direction. The double ellipsoid heat source model is used as the depositing heat source model [12]. The elements of the depositing passes are activated gradually during the depositing process. The inter-pass idle time is 33 s after the deposition of every pass. The initial temperatures of all nodes are set to be the ambient temperature 298K. The mechanical boundary condition is loaded in the principle of no rigid component movement.

The temperature-dependent material properties of the substrate are also used for depositing metal. The material properties adopted at different

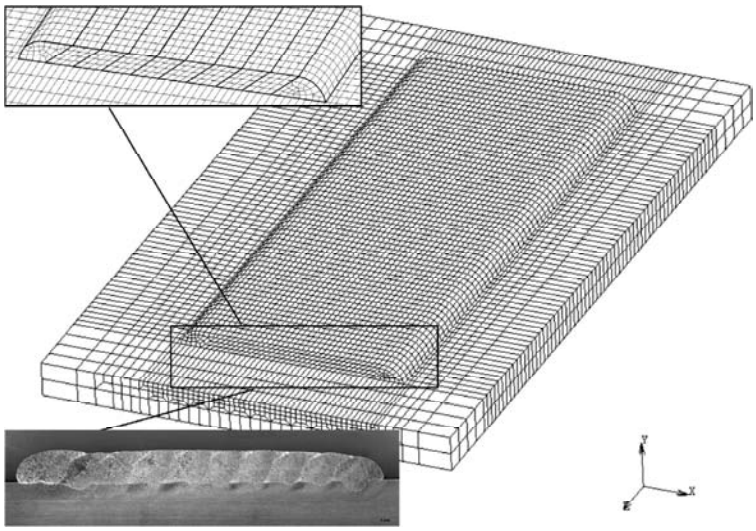

Fig. 4. Three-dimensional finite element model.

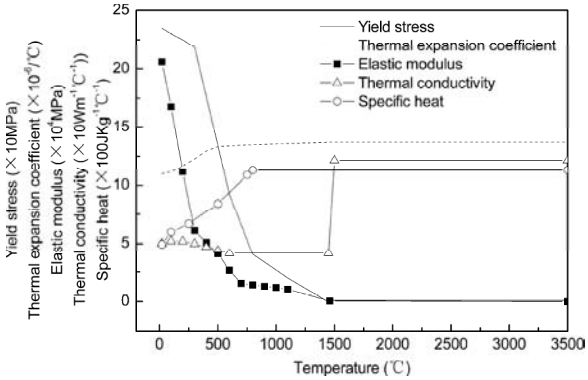

Fig. 5. Material properties at different temperatures.

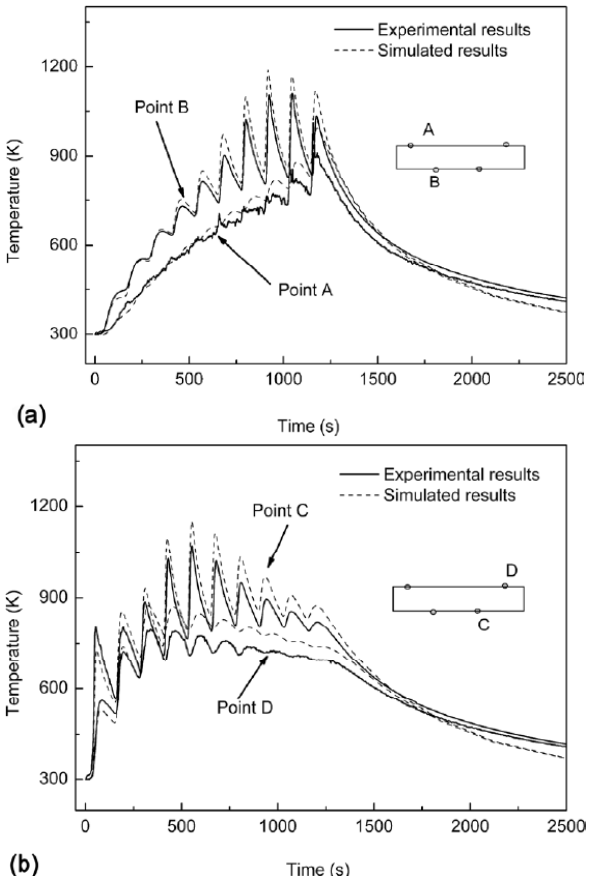

Fig. 6. Simulated and experimental thermal cycles. (a) Points A and B. (b) Points C and D.

temperatures are shown in Fig. 5 [13]. At the ambient temperature, the specific heat is 490 $J \cdot Kg^{-1} \cdot K^{-1}$, and the thermal conductivity is 50.04 $W \cdot m^{-1} \cdot K^{-1}$. The yield stress is 235 MPa, the thermal expansion coefficient is 1.1×10^{-5} K^{-1}, and the Elastic modulus is 2.06×10^5 MPa. The Poisson's ratio is 0.28, the density is 7.85×10^3 $kg \cdot m^{-3}$, and the melting point is 1698K. Above the melting point, the thermal conductivity is artificially increased to compensate for the convection stirring effect in the molten pool [14]. And the combined film coefficient is adopted to consider the general effect of radiation and convection on the surface of weld-based rapid prototyping component [15].

4. RESULTS AND DISCUSSION

4.1. Comparison of simulated and experimental results.

The simulated and experimental results of thermal cycling curves at four points A, B, C, and D are shown in Fig. 6, respectively. The dashed lines are the simulated thermal cycling curves, while the real lines are the experimental results. Both simulated and experimental thermal cycles are multi-peak curves. As shown in the figure, the simulated thermal cycling results are in agreement with the experimental results within normal operating conditions. Comparing the simulated residual stresses along X_1Y_1 with the experimentally measured values, the results are shown in Fig. 7.

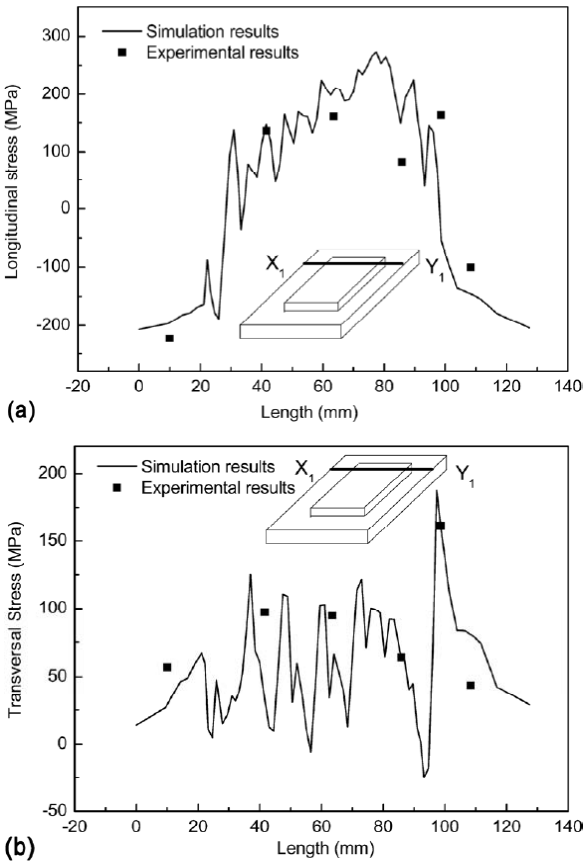

Fig. 7. Simulated and experimental residual stresses. (a) Longitudinal stress. (b) Transversal stress.

The real lines are the simulated results, and the scattered points are the experimental results. The longitudinal stress along X_1Y_1 is shown in Fig. 7a. Longitudinal direction is parallel to the depositing direction. Due to the shrinkage of depositing metal in the cooling stage, the longitudinal tensile residual stress comes into being around depositing metal. The longitudinal compressive stress appears in the region away from the depositing metal. The longitudinal tensile and compressive stresses on this section balance with each other. The transversal residual stress along X_1Y_1 is shown in Fig. 7b. The accordance between the variation trends of simulated and experimental results is acquired. Therefore, the validity of weld-based rapid prototyping numerical model is verified.

4.2. Temperature field and temperature gradient.

Fig. 8 presents the temperature field evolutions, where (a)~(c) are the temperature field distributions of the component when the heat source is respectively at the middle points of the 1st, 5th, and

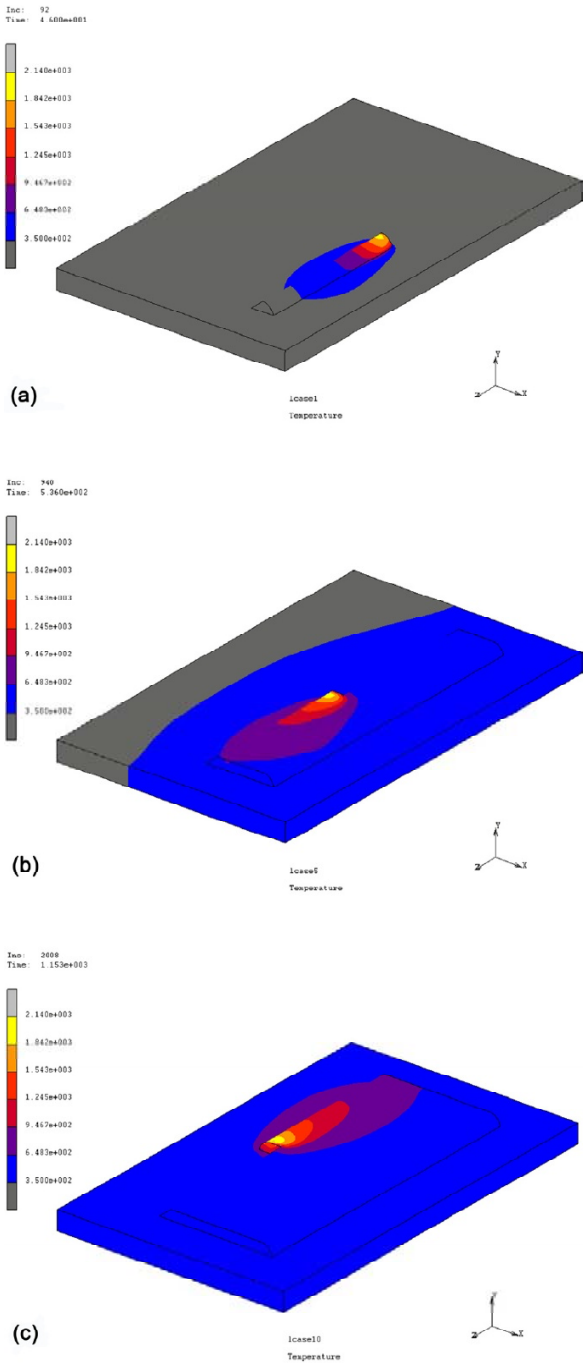

Fig. 8. Temperature field evolutions, when heat source is at middle points of (a) 1st pass, (b) 5th pass, and (c) 10th pass.

10th passes. In the depositing process, the high-temperature region becomes larger and the heat accumulates gradually. The fore pass has pre-heating effect on rear passes and the rear pass has the post-heating effect on fore passes. Fig. 9 shows thermal cycling curves of middle points in the 1st and 3rd passes. There are multiple peaks and wave troughs due to heat treatments experienced. The dashed line stands for the melting point of depositing

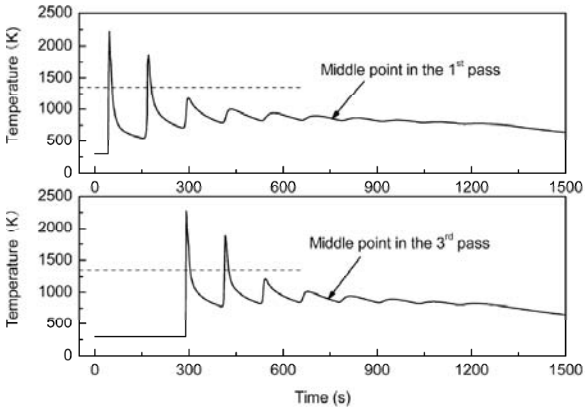

Fig. 9. Thermal cycles of component at middle points of 1st and 3rd passes.

material. As shown, the thermal cycling temperature peaks descend gradually in the depositing process. The wave trough values increase first and then level off gradually. According to the thermal cycling figure, the remelting phenomenon appears, and the metallurgical bonding requirement is satisfied. The thermal cycles at other locations have similar variation regularities.

At one moment, the heat exchanges in the molten pool are as follows:

$$\Delta h_{cum} = \Delta h_{input} - \Delta h_{loss}, \quad (1)$$

where Δh_{cum} is the variation of the heat accumulation in the rapid prototyping process; Δh_{input} is the variation of the heat input; Δh_{loss} is the variation of the heat loss. The heat loss includes the heat conduction to the deposited component h_{cond}, the heat convection to the ambient h_{conv}, and the heat radiation to the ambient h_{rad}. Therefore, Δh_{loss} could be given:

$$\Delta h_{loss} = \Delta h_{cond} + \Delta h_{conv} + \Delta h_{rad}. \quad (2)$$

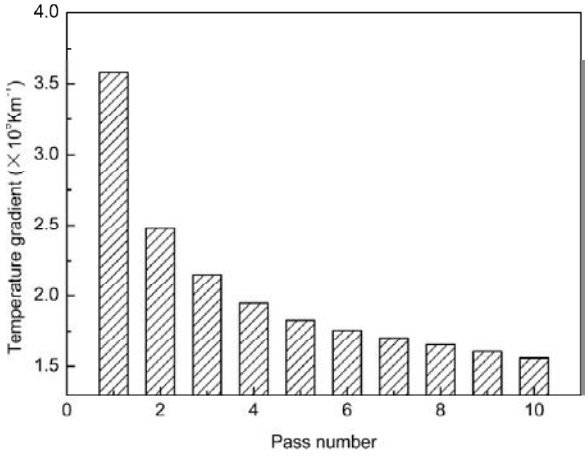

Fig. 10. *Y*-direction maximum temperature gradients in molten pools at middle points of ten passes.

Fig. 10 shows the *Y*-direction maximum temperature gradients in molten pools at middle points of ten passes. The *Y*-direction maximum temperature gradients in the molten pool decrease with the number increase of depositing passes. The maximum value is 3.579×10^5 K·m^{-1}, and the minimum value is 1.560×10^5 K·m^{-1}. Therefore, the heat diffusion condition becomes worse with the number increase of depositing passes, meaning the heat loss h_{loss} decreasing (Δh_{loss} <0). In the depositing process, the heat accumulates and the component temperature increases, resulting in better conditions for the convection and the radiation (Δh_{conv}>0, Δh_{rad} >0). As discussed, the heat loss Δh_{loss} is smaller than zero. Therefore, according to Eq.(2), Δh_{cond} must be smaller than zero, and the absolute value of Δh_{cond} must be larger than the sum of Δh_{conv} and Δh_{rad}. It can be deduced that in the three parts of heat losses, the heat conduction plays a main effect. The descending heat loss of the whole component is mainly resulted by the decreasing heat conduction of depositing passes to the temperature-increasing substrate.

4.3. Von Mises stress evolution

The Von Mises stress evolution of the ten-pass deposition is shown in Fig. 11, where (a)-(d) are the equivalent stress distributions when the heat source locates at the ending points of the 1st, 2nd, 5th, and 10th passes; (e) is the equivalent stress distribution after the component cooling to the room temperature. The equivalent stress of metal in the molten pool is zero. The metal surrounding the molten pool expands due to heating. Therefore, the stresses in the adjacent area are comparatively large. In the depositing process of the 1st pass in the rapid prototyping, the component is first heated and then cools down, resulting in the increase of the equivalent stress. In the depositing process of the 2nd pass, the metal in the 1st pass is reheated even remelted, and there exits a stress release effect of the 2nd pass on the 1st pass. In the whole depositing process, the equivalent stress formed by fore passes is partly released in the post-heating process of rear passes. In the multi-pass rapid prototyping, the two regions on the substrate surrounding the starting and ending arc points are in the comparatively large equivalent stress state. The equivalent stresses surrounding the starting and ending points increase and decrease alternately in the depositing process of multi-pass rapid prototyping. Finally, the equivalent stress of component increases to the equivalent residual stress,

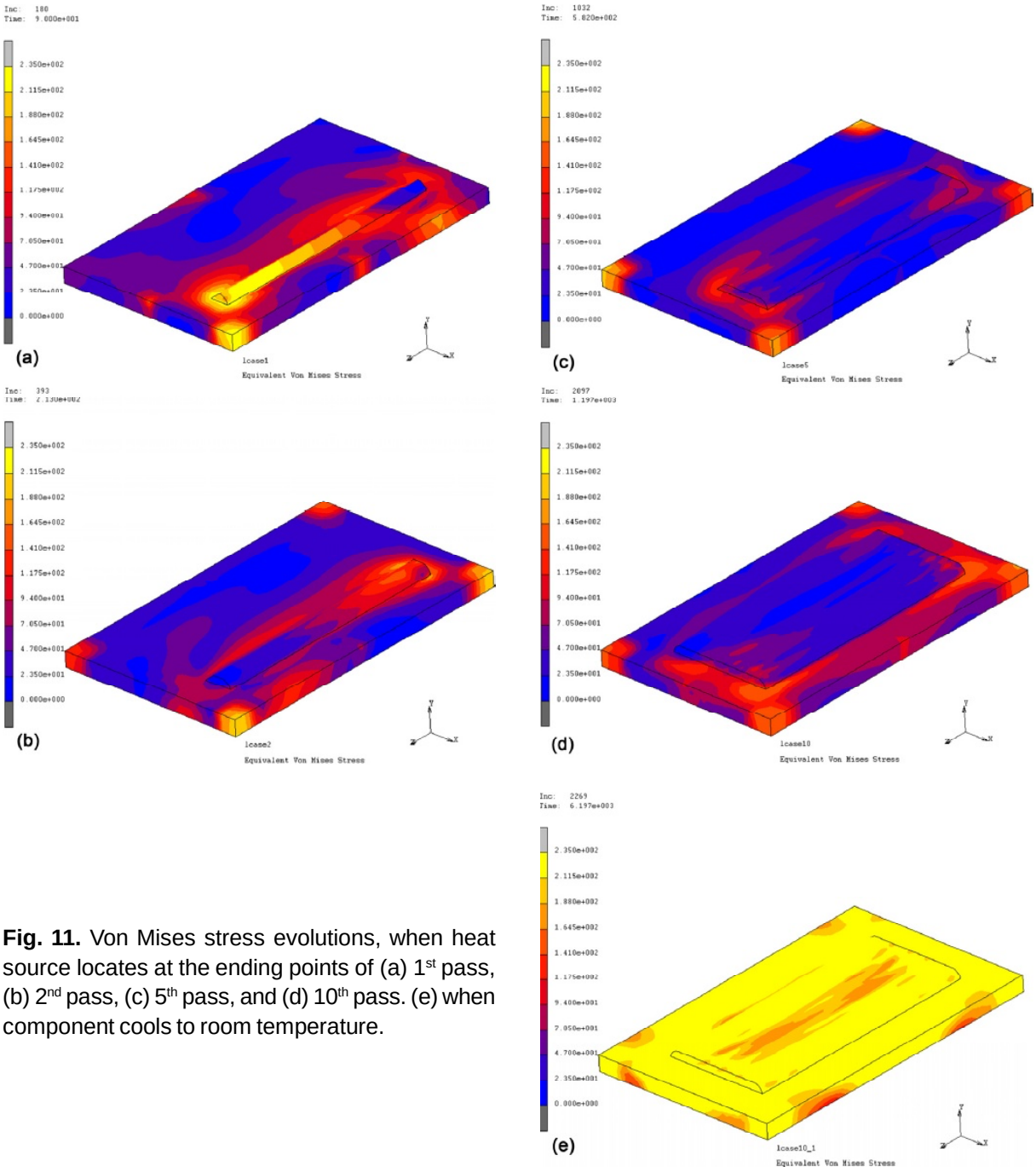

Fig. 11. Von Mises stress evolutions, when heat source locates at the ending points of (a) 1st pass, (b) 2nd pass, (c) 5th pass, and (d) 10th pass. (e) when component cools to room temperature.

when the component cools down to the room temperature, as shown in Fig. 11e. For the depositing metal, residual stresses in the middle region are comparatively low, and residual stresses in the outer region are comparatively high.

The equivalent stress cycle curves in the 1st and 3rd passes are shown in Fig. 12. In the depositing process, there exists the stress release effect of the rear pass on the fore passes. When the heat source passes by the middle point of 1st pass and leaves away, the equivalent stress increases gradually until the deposition of the 2nd pass. The depositing metal of the 1st pass is reheated in the deposition of 2nd pass, and the equivalent stress decreases. The minimum value appears when the metal of the 1st pass is remelted. When the heat source leaves away, the equivalent stress increases again. Finally, the component cools down to the room temperature. The equivalent Von Mises stress comes to the residual stress. The variation regularities of the equivalent stress at the middle point of the 3rd pass are similar. And the local stress peaks at the middle point of the 3rd pass are lower than that at the middle point of the 1st pass due to the stress release ef-

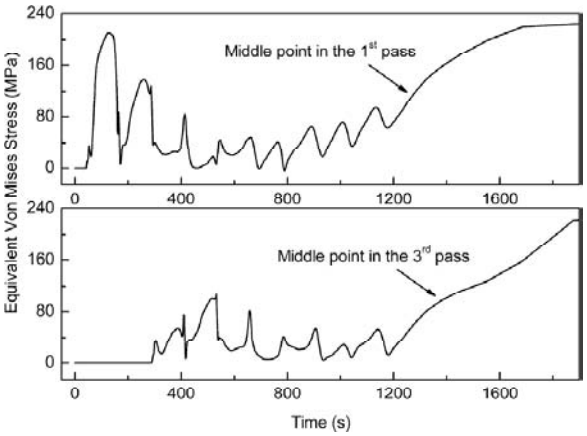

Fig. 12. Equivalent stress cycles of component at middle points of 1st and 3rd passes.

fect. Supposing a point locates at the nth pass, there will be 10-*n*+1 local stress peaks. And finally, when the temperature cools down to the room temperature, the stress comes to the residual stress.

4.4. Inter-pass stress analysis

The inter-pass stresses of different passes along the central line X_2Y_2 of the substrate are shown in Fig. 13. The longitudinal and transverse stresses are observed respectively. In Fig. 13a, large longitudinal tensile stresses distribute in the region of depositing metal due to the shrinkage of cooling stage, whereas in the region away from the depositing metal on the substrate, the longitudinal compressive stress is formed and balances with the longitudinal tensile stress on this section. Among these inter-pass stresses except for that of the tenth pass, the inter-pass stress of the 1st pass is the largest because of the maximum temperature gradient formed in the depositing of the 1st pass. In the rapid prototyping process, the tensile stress peaks decrease gradually after different passes due to the stress release effect of the rear pass on fore passes. When the component cools to the room temperature, the maximum stress, that is the residual stress, comes into being. The main reason for that is that room temperature is much lower than the inter-pass temperatures. In Fig. 13b, the transversal stress along the central line X_2Y_2 is tensile. Among the inter-pass stresses of the front nine passes, the inter-pass transversal stresses decrease gradually. Similarly, the inter-pass stress of the 1st pass is the largest except for that of the tenth pass. When the component cools to room temperature, the inter-pass stress of the tenth pass comes to the maximum, which is the residual stress. Seen from above analysis, the stress of the last

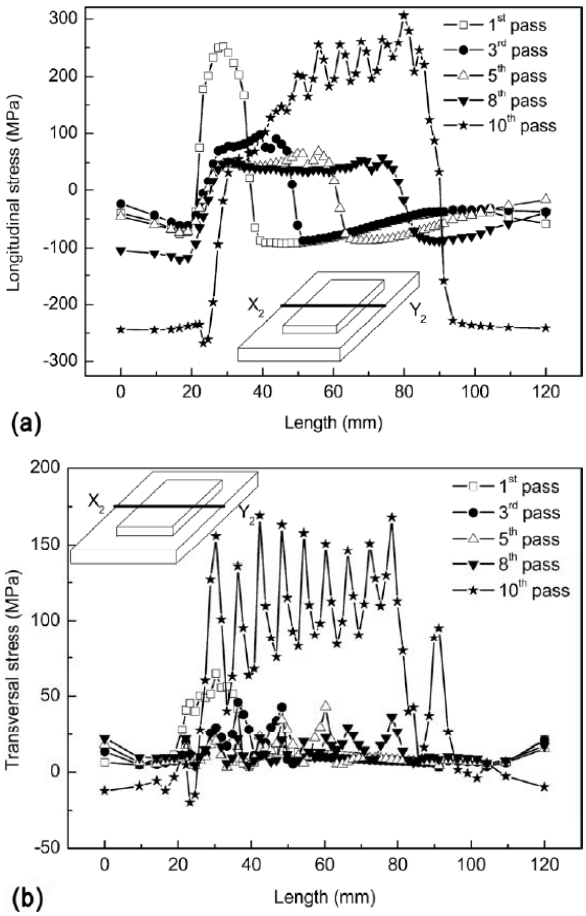

Fig. 13. Inter-pass stresses along central line X_2Y_2 of substrate. (a) Longitudinal stresses. (b) Transversal stresses.

pass plays an important effect in the stress formation of the whole component under the current process parameters.

According to the analysis of temperature field and stress distributions, it can be concluded that the temperature increase of component results in the stress release effect. The non-uniform multi-peak thermal cycle experienced is the main cause of the stress evolutions and distributions in weld-based rapid prototyping.

5. CONCLUSIONS

(1) To verify the finite element model of multi-pass weld-based rapid prototyping, the thermal cycles and residual stresses at concerned locations are measured. After comparing calculated results with the experimental measurements, the agreement of variation trends is acquired.

(2) The component experiences multi-peak thermal cycles. The fore pass has the pre-heating effect on the rear passes, and the rear pass has the post-heating effect on the fore passes. The thermal cy-

cling peaks descend, and the trough values increase first and level off gradually in the depositing process. The inter-pass remelting phenomenon satisfies the inter-pass metallurgical bonding requirement.

(3) In the multi-pass single-layer weld-based rapid prototyping, the heat losses of component mainly include the heat conduction, the heat convection and the heat radiation. The decreasing heat conduction of depositing component plays a main effect, and leads to the decreasing of the whole heat loss of component.

(4) In the multi-pass weld-based rapid prototyping, there exists the stress release effect of rear pass on the fore passes, and the stress of the last pass plays a key effect in the stress formation of the whole component. The main cause of the stress release effect is the non-uniform multi-peak thermal cycle experienced.

ACKNOWLEDGEMENTS

The authors gratefully acknowledge the financial support provided by the National Natural Science Foundation of China under grant No. 50675046, 50775053, and 51175119.

REFERENCES

[1] M.P. Mughal, H. Fawad and R.A. Mufti // *Journal of Mechanical Engineering Science* **220** (2006) 875.

[2] J. H. Ouyang, H. Wang and R. Kovacevic // *Mater. Manuf. Process*. **17** (2002) 103.

[3] Y. M. Zhang, Y. Chen, P. Li and A. T. Male // *J. Mater. Process. Technol*. **135** (2003) 347.

[4] Y. A. Song and S. Y. Park // *J. Mater. Process. Technol.* **171** (2006) 35.

[5] K. Dai and L. Shaw // *Acta Mater.* **49** (2001) 4171.

[6] R. Long, W. Liu, F. Xing and H. Wang // *Trans. Nonferrous Met. Soc. China* **18** (2008) 691.

[7] I.A. Roberts, C.J. Wang, R. Esterlein, M. Stanford and D. J. Mynors // *Int. J. Mach. Tools Manuf.* **49** (2009) 916.

[8] M. Alimardani, E. Toyserkani and J.P. Huissoon // *Opt. Lasers Eng.* **45** (2007) 1115.

[9] A.H. Nickel, D.M. Barnett and F.B. Prinz // *Mater. Sci. Eng. A* **317** (2001) 59.

[10] T. Zhang, C.S. Wu, G.L. Qin, X.Y. Wang and S.Y. Lin // *Comput. Mater. Sci.* **47** (2010) 848.

[11] D. Deng and H. Murakawa // *Comput. Mater. Sci.* **37** (2006) 269.

[12] J. Goldak, A. P. Chakravarti and M. Bibby // *Metal. Trans. B*. **15B** (1984) 299.

[13] D. Gandy, *Carbon Steel Handbook* (EPRI, Palo Alto, California: 1014670, 2007).

[14] L. Lindgren // *J. Therm. Stresses* **24** (2001) 195.

[15] M. Abid and M. Siddique // *Int. J. Pressure Vessels Piping* **82** (2005) 860.